An Immunotherapy Strategy Targeting Programmed Cell Death Ligand 1 and CD73 with Macrophage-Derived Mimetic Nanovesicles to Treat Bladder Cancer

Qidong Zhou
Huashan Hospital Fudan University https://orcid.org/0000-0002-7596-9284
Weihong Ding
Huashan Hospital Fudan University
Zhiyu Qian
Huashan Hospital Fudan University
Quangang Zhu
Shanghai Skin Diseases Hospital
Chuanyu Sun
Huashan Hospital Fudan University
Qin Yu
Shanghai Skin Diseases Hospital
Zongguang Tai
Shanghai Skin Diseases Hospital
Ke Xu (drkexu@163.com)
Huashan Hospital Fudan University https://orcid.org/0000-0001-7222-9523

Research Article

Keywords: macrophage, exosome-mimetic nanovesicles, programmed cell death ligand 1, CD73, immunotherapy, bladder cancer

Posted Date: March 2nd, 2021

DOI: https://doi.org/10.21203/rs.3.rs-256327/v1

Abstract

Background

The tumor microenvironment in bladder cancer exerts an inhibitory effect on immune effector cells. Thus, removing this inhibitory effect could help improve the efficacy of immune checkpoint inhibitors, and combination immunotherapy is a promising strategy for increasing the proportion of patients with bladder cancer who benefit from immune checkpoint inhibitors. However, it is difficult to effectively and simultaneously deliver multiple drugs to the tumor tissue. In this study, we describe the design and in vivo validation of macrophage-derived exosome-mimetic nanovesicles (EMVs) as a nanoplatform for coloading and targeted delivery of a CD73 inhibitor (AB680) and monoclonal antibodies targeting programmed cell death ligand 1 (aPDL1).

Results

Our results indicated that these nanocomplexes (AB680@EMVs-aPDL1) were highly stable, provided adequate biosafety in vivo, and exhibited enhanced targeting in a mouse model of bladder cancer. Moreover, the CD73 inhibitor reduced extracellular adenosine production, and the combination therapy significantly promoted activation of cytotoxic T lymphocytes, resulting in suppression of tumor growth in vivo.

Conclusions

Therefore, using EMVs to deliver a combination of aPDL1 and a CD73 inhibitor may be an effective combined immunotherapy strategy for treating bladder cancer.

Background

Bladder cancer is the 11th most commonly diagnosed cancer, with more than 430,000 new cases and 165,000 related deaths each year [1, 2]. Approximately 20–25% of patients with bladder cancer present with muscle-invasive bladder cancer (MIBC) or metastatic bladder cancer [3]. During the last two decades, platinum-based combination chemotherapy has been the first-line treatment for MIBC after radical cystectomy and for metastatic bladder cancer [4], although the curative rate is still unsatisfactory [5, 6]. Immune checkpoints inhibitors (ICIs) have recently emerged as an effective option for treating various cancers [7]. Bladder cancer has the third highest mutation burden among all cancers, which may increase the neoantigen load, enhance immunogenicity, and ultimately improve the response to immunotherapy [8, 9]. Since 2016, various monoclonal antibodies (mAbs) that target programmed cell death 1 (PD-1) or programmed cell death ligand 1 (PD-L1) have been approved and clinically used to treat cisplatin-resistant and metastatic MIBC [10]. Although ICI treatment of MIBC can provide good efficacy in some cases, the objective response rate is approximately 20% [11–13], highlighting the challenges of effective immunotherapy for advanced and metastatic MIBC.

Cancer cells achieve immune escape through various mechanisms, which may decrease the effectiveness of blocking immune checkpoints. Thus, combined immunotherapy is a promising strategy for increasing the proportion of patients with MIBC who objectively benefit from ICIs. One promising approach to overcoming ICI resistance involves eliminating the inhibitory effect of the tumor microenvironment (TME) on immune effector cells [14]. In this context, the TME produces various immunosuppressive factors and elevated adenosine levels strongly inhibit tumor-reactive T-cells and natural killer cells [15]. The main source of adenosine is the decomposition of AMP by CD73 (an ecto-5' nucleotidase), which is highly expressed on the surface of immune cells and cancer cells [16]. Furthermore, the CD73-adenosine metabolic pathway plays an important role in immunosuppression and is associated with a poor prognosis in many solid tumors [17, 18]. Moreover, anti-PD-1/PD-L1 treatment may increase CD73 expression on cancer cells and attenuate the effects of treatment [19]. However, targeting CD73 can inhibit the development and metastasis of multiple tumor types and cause synergistic effects with anti-PD-1/PD-L1 treatment [20, 21]. Therefore, in our laboratory, we have investigated strategies to combine anti-PD-L1 treatment (aPDL1) with CD73 inhibitors, such as AB680, to enhance immunotherapeutic effects in patients with bladder cancer [22].

The synergistic effects of this combined strategy may require the simultaneous delivery of aPDL1 and AB680 to concurrently exert their effects on tumor tissues. In this context, improving nanotechnology may help guide the development of more rational and effective drug delivery systems [10], which could permit simultaneous, sustained, and targeted delivery. Exosome-mimetic nanovesicles (EMVs), which are prepared via serial cell extrusion, have recently been considered as an alternative to extracellular vesicles as nanodrug systems [23, 24] because they share similar characteristics, including the membrane properties of the parent cell [25]. Furthermore, relative to extracellular vesicles, EMVs are less expensive to prepare and have a greater production yield with more enrichment of proteins and RNAs [26, 27]. Moreover, EMVs can be engineered to have enhanced drug/gene loading efficiency and better targeted delivery or diagnostic functions [28, 29]. Thus, macrophage-derived EMVs have been used as tumor-targeting vehicles to simultaneously deliver mAbs and small molecule inhibitors [23, 30, 31].

In the current study, we designed and validated a nanoplatform for treating bladder cancer using macrophage-derived EMVs to simultaneously deliver aPDL1 and AB680 as combined immunotherapy. The EMVs were derived from a macrophage cell line (RAW264.7 cells), and AB680 was encapsulated into the EMVs (AB680@EMVs) using a co-extrusion method. The aPDL1 was then conjugated to the surface of the EMVs (AB680@EMVs-aPDL1) in order to enhance tumor accumulation and therapeutic effects (Scheme 1). In vitro and in vivo models were used to evaluate the tumor-targeting and therapeutic effects of this nanodrug system as a combined immunotherapy strategy for treating bladder cancer.

Materials And Methods

Materials

AB680 and aPDL1 (atezolizumab) were obtained from MedChemExpress (NJ, USA). Nile Red and 1.1'-dioctadecyltetramethyl indotricarbocyanine iodide (DiR) were purchased from Solarbio (Beijing, China). Dimethyl sulfoxide (DMSO) and 4',6-diamidino-2-phenylindole (DAPI) were obtained from Sigma-Aldrich (St. Louis, MO, USA). The Cell Counting Kit-8 (CCK-8) and bicinchoninic acid (BCA) Protein Assay Kit were obtained from Beyotime (Nanjing, China). Enzyme-linked immunosorbent assay (ELISA) kits for tumor necrosis factor alpha (TNF-α) and interferon gamma (IFN-γ) were obtained from R&D Systems (Minneapolis, MN, USA). Antibodies targeting mouse CD4, CD8, and CD69, as well as carboxyfluorescein diacetate succinimidyl ester (CFDA-SE) and propidium iodide (PI), were purchased from BD Biosciences (San Diego, CA, USA). DSPE-PEG_{2000}-NHS (2,990 Da) was obtained from Nanosoft Polymers (Winston-Salem, NC, USA). Dynabead kits targeting mouse $CD8^+$ cells and mouse T-activator CD3/CD28 were purchased from ThermoFisher (Waltham, MA, USA). An Adenosine Assay Kit, anti-mouse Ki-67 primary antibodies, and goat anti-human secondary antibodies were purchased from Abcam (Cambridge, UK). All reagents and chemicals were of analytical grade.

Cell lines and animals

MB49 cells (murine transitional cell carcinoma of the bladder) was obtained from the Chinese Academy of Sciences Cell Bank (Shanghai, China). RAW264.7 cells (murine macrophages) were obtained from the China Centre for Type Culture Collection (Wuhan, China). MB49 and RAW264.7 cells were cultured in RPMI 1640 medium (Invitrogen, Carlsbad, CA, USA) supplemented with 10% fetal bovine serum (FBS) and 1% penicillin-streptomycin (Gibco) at 37°C in an atmosphere containing 5% CO_2.

Male C57BL/6J mice (5–6 weeks old, weight: 15–18 g) were purchased from the Shanghai SLAC Laboratory Animal Co., Ltd. (Shanghai, China) and were housed under specific pathogen-free conditions. All animal experiments were approved by the animal care and use committee of Fudan University and conformed to the National Research Council guidelines for Laboratory Animal Care in Research.

Preparation of AB680@EMVs and AB680@EMVs-aPDL1

A stock solution of AB680 (1 mg/mL) was prepared in DMSO. The EMVs were prepared using slight modifications of previously reported protocols [32, 33]. RAW264.7 cells were resuspended at a density of 5×10^6 cells/mL in Dulbecco's phosphate-buffered saline (PBS) with different concentrations of AB680 and then serially extruded through polycarbonate membrane filters with varying pore sizes (5, 1, 0.4, and 0.2 μm; Millipore Isopore) using a mini extruder. The co-extrusion product was centrifuged (40,000 × *g* at 4°C for 1 h) to remove debris and unbound AB680.

aPDL1 was conjugated to AB680@EMVs using DSPE-PEG_{2000}-NHS as a crosslinker and the postinsertion method. PEG-DSPE block copolymers are amphiphilic polymers that are used to prepare various types of nanomaterials, and the PEG terminal groups can be activated and connected to various targeting ligands. The postinsertion method is a simple, rapid technique used to insert various drug ligand-PEG-DSPE copolymers into nanoparticles [34, 35]. aPDL1 (2 mg/mL in borate buffer, pH 8.0) was incubated with DSPE-PEG_{2000}-NHS (dissolved in DMSO) at a molar ratio of 1:10 and stirred gently for 6 h at room

temperature. The excess DSPE-PEG_{2000}-NHS was removed using dialysis (molecular weight: 3,500 Da), and the remaining aPDL1-PEG-DSPE was reacted with EMVs or AB680@EMVs at various molar ratios for 2 h. To eliminate unconjugated antibodies, the resulting mixture was centrifuged at 40,000 rpm for 30 min and then washed twice using borate buffer. After centrifugation, the supernatant was scanned to determine the surface-bound antibody concentration, which was calculated as the original amount minus the free antibody concentration in the supernatant. The AB680@EMVs-aPDL1 were then redispersed in PBS (pH 7.4).

Characterization of AB680@EMVs and AB680@EMVs-aPDL1

The particle size, zeta potential, and polymer dispersion index of the EMVs, AB680@EMVs, and AB680@EMVs-aPDL1 were characterized using dynamic light scattering at 25°C (Zetasizer Nano ZS90; Malvern). The size stability of the AB680@EMVs-aPDL1 in PBS and 10% serum was also measured at different time points using dynamic light scattering. The morphology of the AB680@EMVs and AB680@EMVs-aPDL1A was evaluated using transmission electron microscopy (TEM; JEM2100, Japan) at an acceleration voltage of 75 kV.

The presence of aPDL1 on the EMVs was identified using secondary antibodies (fluorescein isothiocyanate [FITC]-labeled goat anti-human immunoglobulin). The secondary antibodies (100 μL) were incubated for 2 h at room temperature with 2 mL of the AB680@EMVs-aPDL1 or AB680@EMVs dispersions, which were then centrifuged to remove the excess antibodies and washed twice. The stained nanocomplexes were then redispersed in PBS at pH 7.4, and fluorescence was evaluated using fluorescence microscopy (BX-60F; Olympus, Japan).

The protein concentrations in the EMVs were quantified using the BCA method. The EMV solution was diluted 10-fold using acetonitrile, sonicated for 30 min, and filtered using a 0.45-μm membrane. The amount of AB680 in the EMVs was analyzed using high-performance liquid chromatography at 225 nm (Agilent Technologies, CA, USA). Chromatography was performed using a C18 column (5 μm, 250 × 4.6 mm) at 40°C with 25% acetonitrile and 75% purified water containing 10 mM K_2HPO_4 (pH 5.3) and 0.15 mM ethylenediaminetetraacetic acid as the mobile phase, which was pumped at a rate of 1.0 mL/min. Drug loading was calculated as the amount of AB680 divided by the amount of EMV protein (nm/μg). The encapsulation efficiency was calculated as the amount of AB680 present in the EMVs divided by the total amount of AB680. The amount of bioactive aPDL1 conjugated to the EMVs was calculated based on the difference between the original amount and the amount in the supernatant using the BCA method. The graft ratio was calculated as the amount of conjugated-aPDL1 divided by the total amount of aPDL1.

In vitro release of AB680 from the EMVs

The in vitro release of AB680 from the AB680@EMVs and AB680@EMVs-aPDL1 was evaluated over a 48-h period using a dialysis bag at 37°C. Each sample (3 mL) was added to a separate dialysis bag

(molecular weight: 1,000 Da), which was immersed in 30 mL of a release medium (PBS [pH 7.4] or acetate buffer [pH 5.5]) with gentle agitation. At the predetermined time intervals, 2 mL of the release medium were removed for analysis and replaced with an equivalent volume of fresh medium. The concentration of AB680 in the removed medium was measured using high-performance liquid chromatography and the chromatographic conditions described above.

In vitro cellular uptake

Flow cytometry was used to assess cellular uptake of the EMVs, and Nile Red was used as a substitute for AB680 in Nile Red@EMVs and Nile Red@EMVs-aPDL1. MB49 cells were harvested, seeded into 12-well plates (5×10^5 cells/well), and cultured for 24 h at 37°C. The medium was then replaced with fresh medium containing the Nile Red@EMVs or Nile Red@EMVs-aPDL1 (Nile Red at 50 ng/mL), and the cells were cultured for 2 h. The medium was then removed, MB49 cells were collected, and flow cytometry was performed (Attune NxT; Thermo, USA). These experiments were performed in triplicate.

Confocal laser scanning microscopy was also used to evaluate the cellular uptake and distribution of Nile Red@EMVs-aPDL1. MB49 cells were inoculated into glass-covered 24-well plates (5×10^4 cells/well) and cultured for 24 h. The medium was then replaced with serum-free medium containing free Nile Red, Nile Red@EMVs, or Nile Red@EMVs-aPDL1 (Nile Red at 50 ng/mL). The cells were cultured for 2 h, the medium was discarded, and the cells were washed three times using PBS before being immediately fixed in precooled 4% paraformaldehyde for 30 min. Finally, MB49 cells were stained using DAPI as a nuclear dye and visualized using confocal laser scanning microscopy (FV100; Olympus).

Inhibition of extracellular adenosine production

MB49 cells were cultured in 24-well plates under standard conditions. On the day of the experiment, the cells were pretreated for 4 h using 0.5 mL medium containing different concentrations of AB680, AB680@EMVs, and AB680@EMVs-aPDL1. The cells were then washed twice and incubated for 1 h in 0.5 mL PBS. The extracellular adenosine concentrations for each group were determined using an Adenosine Assay Kit according to the manufacturer's instructions.

In vitro T-cell activation

Purified $CD8^+$ T cells were obtained from splenocytes that had been isolated from C57BL/6J mice (5–6 weeks old) via negative separation selection using a Dynabeads kit for mouse $CD8^+$ cells, according to the manufacturer's instructions. The $CD8^+$ T cells were then seeded into 96-well plates (1×10^5 cells/mL, 0.2 mL/well) and stimulated using Dynabeads mouse T-activator CD3/CD28 (2 μL/well). The cells were then cultivated for 24 h with PBS, AB680, or AB680@EMVs (equivalent to AB680 at 5 nM), and CD69 expression was measured using phycoerythrin-conjugated antibodies to mouse CD69 using flow cytometry.

In vitro coculture

MB49 cells were collected in the logarithmic phase and stained using CFDA-SE (5 μM) at 37°C for 10 min. CFDA-SE-labeled cells were then washed twice using PBS and resuspended in RPMI-1640 medium to a final concentration of 1×10^5 cells/mL. Unlabeled splenocytes were also suspended in RPMI-1640 medium (5×10^6 cells/mL) to act as effector cells against CFDA-SE-labeled MB49 cells. CFDA-SE-labeled MB49 cells were plated in 12-well plates (1×10^5 cells/mL, 0.5 mL/well), and the splenocytes (5×10^6 cells/mL, 0.5 mL/well) were then added to plates to produce a 50:1 ratio of effector:target cells. The target cells were also incubated without effector cells to evaluate spontaneous cell death. After incubation for 4 h, the mixture of cells was treated for 24 h using different complexes (equivalent to 3 μg/mL of aPDL1 or AB680 at 5 nM) or PBS as a control. The cells were then collected and stained using PI, and MB49 cell death (ratio of CFDA-SE^+/PI^+) was evaluated after CFDA-SE-labeled tumor cells were gated using flow cytometry [36, 37].

In vivo biodistribution

A near infrared fluorescent dye (DiR) was used to replace AB680 in traceable DiR@EMVs-aPDL1, which were used for the biodistribution analysis. A mouse model of bladder cancer was created by subcutaneously injecting MB49 cells (2×10^6 cells/200 μL) into the right lateral chest wall of C57BL/6J mice. Tumor-bearing mice were then intravenously injected with free DiR or DiR@EMVs-aPDL1 (equivalent to 5 mg/kg of DiR) via the tail vein. After 24 h, the mice were sacrificed, and the main organs and tumor tissues from each group were collected for ex vivo fluorescent imaging using an optical and X-ray live imaging system (Bruker; excitation: 760 nm, emission: 790 nm).

In vivo synergistic antitumor effects

The in vivo antitumor effects of the AB680@EMVs-aPDL1 were evaluated using tumor-bearing C57BL/6J mice. When the tumor size reached approximately 100 mm^3, the mice were randomly divided into seven groups (6 mice/group), and the day of randomization was defined as day 0. Tumor-bearing mice were intravenously injected four times every 3 days (four injections over a 9-day period) with PBS (control group), EMVs, AB680, aPDL1, AB680@EMVs, EMVs-aPDL1, or AB680@EMVs-aPDL1 via the tail vein. The doses were 5 mg/kg of aPDL1 and 10 mg/kg of AB680. However, because atezolizumab is a human IgG1, the four injections for that group were administered over a shorter period (i.e., days 1, 4, 7, and 10) to avoid the development of neutralizing mouse anti-human immunoglobulin [38]. The lengths and widths of the tumors were measured every 3 days using calipers, and the mice were also weighed. The tumor volume (mm^3) was calculated as $width^2 \times length / 2$. After day 15, all mice were euthanized, and the tumors were excised and weighed.

In vitro and in vivo safety assessment of EMVs

The cytotoxic effects on MB49 cells were evaluated using CCK8 assays. MB49 cells were seeded into 96-well plates (5×10^3 cells/well) and cultured for 24 h before treatment using PBS (control group), EMVs, AB680, aPDL1, AB680@EMVs, EMVs-aPDL1, or AB680@EMVs-aPDL1 (equivalent to 3 μg/mL aPDL1 and

5 nM AB680). After 24 h of incubation, the numbers of viable cells were determined using CCK-8 assays according to the manufacturer's instructions. Untreated control cells were considered 100% viable.

Mice were also treated using different products and then sacrificed on day 15. The main organs (heart, liver, spleen, lungs, and kidneys) were immediately collected and fixed using 4% paraformaldehyde for 1 day. The tissues were then embedded in paraffin, sliced into 5-μm sections, and stained using hematoxylin and eosin for histological evaluation.

Ki-67 expression and immunohistochemical analysis of tumor tissues

The antitumor effects of the EMVs were also evaluated based on the expression of Ki-67 (a marker of tumor cell proliferation) in the tissues. After the mice were sacrificed, the tumors were harvested, washed, fixed, and subjected to hematoxylin and eosin staining and immunostaining to detect Ki-67 expression (primary antibody, 1:100 dilution), as previously reported [28, 39, 40]. The slices were then examined using an inverted light microscope (H550S; Nikon, Japan) by a certified pathologist who was blinded to the sample status.

Immunological analysis of tumor-infiltrating lymphocytes

The tumors were sectioned into small pieces (1–2 mm^3) after necrotic and connective tissues had been removed. The small pieces were gently squeezed through a 200-mesh nylon sifter and then repeatedly ground and rinsed using PBS to acquire tumor-infiltrating lymphocytes (TILs), which were collected as a single-cell suspension. In a sterile centrifuge tube, 3 mL mouse lymphocyte separation solution was placed in layers of 100% (density: 1.083 g/mL) and 75% (density: 1.062 g/mL), and then 3 mL of the collected cell suspension was added before centrifugation at 2,000 rpm for 5 min. The enriched TIL suspension in the 100% layer was collected, washed with buffer, adjusted to an appropriate density, and then incubated with phycoerythrin-conjugated antibodies to mouse CD4 and allophycocyanin-conjugated antibodies to mouse CD8 antibodies for 30 min at room temperature. Flow cytometry was then performed to determine the $CD8^+/CD4^+$ ratio for the TILs.

Tumor-associated cytokine concentrations

Tumor tissues were finely ground in liquid nitrogen and then dissolved for 20 min in RIPA buffer containing 1 mM phenylmethylsulfonyl fluoride. The supernatants were collected via centrifugation (12,000 × *g*) at 4°C for 30 min. Concentrations of TNF-α and IFN-γ in the supernatants were evaluated using corresponding ELISA kits according to the manufacturer's instructions.

Statistical analysis

All analyses were performed using GraphPad Prism 8.0 (SanDiego, CA, USA). Experimental data were presented as means ± standard deviations. Two groups were compared using Student's unpaired t tests, and multiple groups were compared using one-way analysis of variance. Results with *P* values less than 0.05 were considered statistically significant.

Results And Discussion

Characterization of the AB680@EMVs-aPDL1

The characteristics of the EMVs, AB680@EMVs, and AB680@EMVs-aPDL1 are summarized in Fig. 1 and Table 1. AB680@EMVs-aPDL1 had a mean diameter of 218.2 ± 17.6 nm and a polydispersity index of 0.108 ± 0.013. Dynamic light scattering analysis revealed that the mean hydrodynamic diameter of the AB680@EMVs-aPDL1 increased after drug loading and antibody conjugation (Fig. 1A, B). Similarly, the zeta potential for AB680@EMVs-aPDL1 decreased from − 9.4 to − 13.7 mV (compared with AB680@EMVs), which may reflect the presence of the negatively charged aPDL1-PEG-DSPE. The sizes of the AB680@EMVs-aPDL1 and AB680@EMVs suggested that these complexes were reasonable for systematic administration, based on the enhanced permeability and retention effect [41, 42]. Furthermore, serial extrusion through polycarbonate membranes with varying pore sizes reportedly provides 8-fold greater EMV production with 26-fold greater total protein content versus natural exosomes [43].

The morphological characteristics of AB680@EMVs-aPDL1 were observed using TEM, which revealed a generally spherical and compact shape (Fig. 1B). AB680@EMVs-aPDL1 did not exhibit any clear differences compared with blank EMVs, although the edge intensity of the AB680@EMVs-aPDL1 appeared to be increased. Moreover, AB680@EMVs-aPDL1 maintained sizes of 200–230 nm for up to 72 h in PBS (pH 7.4) and in PBS with 10% FBS (Fig. 1C), with no significant differences between the two types of media, suggesting that these complexes had stable sizes that were appropriate for clinical applications. Fluorescence microscopy revealed circumferential green fluorescence (Fig. 1D), which indicated binding of the FITC-labeled secondary antibodies around the AB680@EMVs-aPDL1 and suggested that aPDL1-PEG-DSPE was successfully distributed around the EMVs.

As shown in Table 1, AB680@EMVs-aPDL1 were successfully prepared with a high encapsulation efficiency (61.0% ± 3.1%). Furthermore, loading of AB680 into the EMVs and EMVs-aPDL1 increased at AB680 concentrations of 30–90 μM (Fig. 1E), although no additional loading was observed at concentrations greater than 90 μM, suggesting that the optimal loading concentration was 90 μM. The AB680 content decreased slightly after insertion of aPDL1-PEG-DSPE into AB680@EMVs-aPDL1, which may be related to AB680 release during the conjugation process (Table 1, Fig. 1E). We also investigated the graft ratio of aPDL1 conjugated on the surface of the EMVs using a series of EMVs/aPDL1 weight ratios (1.0–3.5 mg protein/mg, w/w; Table 2). A ratio of 2.5 mg protein/mg (w/w) was ultimately selected to synthesize the EMVs-aPDL1 for subsequent experiments.

In vitro kinetics of AB680 release from the EMVs

Because characterization of the EMVs suggested that these vesicles had good stability, we also evaluated AB680 release at normal physiological pH (pH 7.4, PBS) and in an acidic environment (pH 5.5, acetate buffer). The in vitro drug release profile of the AB680-loaded EMVs-aPDL1 was evaluated over 48 h (Fig. 1F), which revealed a burst of AB680 release during the first 12 h and a more constant sustained release during the next 36 h. These results suggested that the EMVs could provide a sustainable drug

concentration within the tumor site. In addition, the EMVs released approximately 50% of AB680 at normal physiological pH, with an increase to 65% in the acidic environment, which may be explained by EMV aggregation and structural disruption in the acidic environment. This property may also be considered desirable for cancer therapy, given the acidic nature of the TME [30, 44]. Our results indicated that the AB680@EMVs and AB680@EMVs-aPDL1 could maintain continuous release of a CD73 inhibitor for up to 2 days, with improved release in an acidic environment.

Cellular uptake of AB680@EMVs-aPDL1

Flow cytometry was used to evaluate uptake of AB680@EMVs-aPDL1 by MB49 cells using Nile Red as a substitute for AB680. The Nile Red@EMVs group had significantly greater fluorescence after 2 h, relative to the group with free Nile Red ($P < 0.01$; Fig. 2A, B), although the uptake profiles of Nile Red@EMVs-aPDL1 and Nile Red@EMVs were similar ($P > 0.05$). Intracellular colocalization of the EMVs was investigated using confocal laser scanning microscopy, which also revealed that Nile Red@EMVs-aPDL1 or Nile Red@EMVs had much greater fluorescence around DAPI-stained nuclei, relative to free Nile Red (Fig. 2C). In this context, a membrane surface with good biocompatibility is critical for nanocomplexes. Furthermore, macrophage-derived EMVs have good ability to target tumor cells [23, 30]; AB680 internalization is thought to occur via passive diffusion, and cellular uptake of EMVs is thought to involve clathrin-mediated endocytosis and macropinocytosis [45]. Although MB49 cells strongly express PD-L1 [38], which facilitates the binding of EMVs-aPDL1, the negative charge and relatively large size of EMVs may impair uptake to some extent [46]. Nevertheless, our findings suggested that the AB680@EMVs-aPDL1 had good in vitro cellular uptake.

Inhibition of extracellular adenosine production

The inhibitory effects of free AB680, AB680@EMVs, and AB680@EMVs-aPDL1 on CD73 in MB49 cells were evaluated based on extracellular adenosine production. In tumor cells, CD39 and CD73 work in tandem to generate extracellular adenosine, which triggers the accumulation of immunosuppressive intracellular cAMP in antitumor T cells via signaling through high-affinity receptors (A2AR) and low-affinity receptors (A2BR) [47, 48]. We pretreated MB49 cells using different concentrations of AB680, AB680@EMVs, and AB680@EMVs-aPDL1, and an Adenosine Assay Kit was then used to evaluate adenosine production over a 1-h period. Adenosine production was inhibited in a concentration-dependent manners by free AB680, AB680@EMVs, and AB680@EMVs-aPDL1 (Fig. 3A), with clearly higher inhibition observed after pretreatment using AB680@EMVs and AB680@EMVs-aPDL1 (compared with free AB680, $P < 0.01$). This may be related to the greater cellular uptake of AB680 by EMVs. Although the measured adenosine concentrations were slightly lower in the AB680@EMVs-aPDL1 group than in the AB680@EMVs group, the difference was not statistically significant.

Enhanced in vitro T-cell activation

As an early marker of lymphocyte activation, CD69 expression can be used to estimate the activation of $CD8^+$ T cells [49]. Because T-cell activation requires costimulatory signals, mouse T-activator CD3/CD28 was used before the various treatments. We observed that AB680 and AB680@EMVs strengthened T-cell

activation in vitro (Fig. 3B, C), with AB680@EMVs having a clearly stronger effect ($P < 0.05$). In the TME, CD73 is expressed by many cell types (including T lymphocytes) [16]. The control group also had clearly reduced CD69 expression ($P < 0.01$), indicating that AB680 suppression of the CD73-adenosine signaling pathway via EMVs may be instrumental for removing local immunosuppression.

In vitro antitumor effects

We created a coculture system of CFDA-SE-labeled MB49 cells and splenocytes isolated from C57BL/6J mice (50:1 ratio) and used flow cytometry to evaluate the cytotoxic effects of various treatments on MB49 cells. Relative to the control group, the culture medium (PBS) group exhibited mild cytotoxic effects (Fig. 3D, E), exerted by the mouse-derived splenocytes. However, the AB680 and AB680@EMVs groups had significantly less cytotoxic effects, relative to the aPDL1 and EMVs-aPDL1 groups ($P < 0.01$), whereas the AB680@EMVs-aPDL1 group had strong cytotoxic effects relative to the aPDL1 group ($P < 0.01$) and the EMVs-aPDL1 group ($P < 0.05$). Thus, although AB680 or AB680@EMVs alone could enhance the cytotoxic effects of lymphocytes via reduced extracellular adenosine production, their effects were clearly lower than those of aPDL1 or EMVs-aPDL1, and AB680@EMVs-aPDL1 exerted even greater cytotoxic effects. Therefore, AB680 appeared to exert synergistic effects with aPDL1 treatment.

In vivo biodistribution of the EMVs

The tumor-targeting ability of AB680@EMVs-aPDL1 was evaluated using C57BL/6J mice bearing MB49-derived tumors. The EMVs were labeled using DiR dye, and in vivo biodistribution was evaluated using the main organs and tumor after 24 h of treatment. The free DiR was metabolized mainly by the liver and kidneys, with no clear tumor accumulation (Fig. 4), although clear tumor accumulation was observed in the DiR@EMVs-aPDL1 group. This may be explained by the enhanced permeability and retention effect, which allows nanoparticles to passively accumulate at the tumor site, rather than in normal tissues [41, 42, 50]. Furthermore, macrophage membranes contain chemoattractant proteins, which are retained in the EMVs, to facilitate homing to the tumor site. Therefore, the EMVs may be able to accumulate in bladder tumors.

In vivo tumor inhibition and histological analyses

The mouse model was used to evaluate the in vivo therapeutic efficacy of AB680@EMVs-aPDL1 and other treatments (four injections, typically over a 9-day period), based on changes in body weight and tumor volume. The PBS and EMV groups did not exhibit any significant antitumor effects (Fig. 5A, B), although variable reductions in tumor growth were observed in the groups that received AB680, AB680@EMVs, aPDL1, EMVs-aPDL1, and AB680@EMVs-aPDL1. In this context, previous studies have indicated that CD73 inhibitors, particularly when combined with ICIs, could limit the growth of various tumors [19, 20, 51]. Similarly, we observed that AB680 and AB680@EMVs had antitumor effects in a model of bladder cancer, and the greater effect of AB680@EMVs ($P < 0.05$) may be related to targeted accumulation of EMVs at the tumor site. However, the inhibitory effects of AB680@EMVs were weaker than those of aPDL1 and EMVs-aPDL1 ($P < 0.01$), and the greatest inhibitory effect was observed in the AB680@EMVs-aPDL1 group (average day 15 tumor volume: 405.1 mm^3, $P < 0.01$). Moreover, the

AB680@EMVs-aPDL1 group had a significantly lower tumor weight on day 15, consistent with the tumor volume curve (Fig. 5C, $P < 0.01$). Thus, codelivery of aPDL1 and AB680 via the EMVs appeared to exert potent synergistic effects against an in vivo model of bladder cancer.

We also performed immunohistochemical staining of tumor specimens, revealing dense cell arrangements with complete structures and clear nuclear and cellular outlines in the control and EMV groups (Fig. 5D). However, clear cellular disruptions were observed in tumors that had been treated using aPDL1, EMVs-aPDL1, AB680@EMVs, and AB680@EMVs-aPDL1. Furthermore, AB680@EMVs-aPDL1 treatment reduced the expression of Ki-67 (a major indicator of tumor progression) [52, 53].

Mechanisms of tumor suppression

Tumor cells escape immune surveillance and clearance through the binding of PD-L1 to PD-1 on the surface of T lymphocytes [54]. In addition, CD73-mediated adenosine signaling through A2AR helps drive the transition of naïve/memory $CD8^+$ T cells into effector cells via suppression of Wnt signaling [55, 56]. The antitumor mechanism of AB680@EMVs-aPDL1 treatment was evaluated using flow cytometry to examine the proportion of $CD8^+/CD4^+$ TILs, because a higher $CD8^+/CD4^+$ ratio in bladder cancer predicts a better response to PD-1 inhibition and greater tumor regression [57]. Relative to the control group, aPDL1 treatment increased the amount of $CD8^+$ TILs, and AB680 treatment also exerted similar effects (Fig. 6A, B). The highest $CD8^+/CD4^+$ ratio was observed in the AB680@EMVs-aPDL1 group, which also had the greatest therapeutic effect.

The intratumoral concentrations of TNF-α and IFN-γ were estimated in all groups. Relative to the control group, the AB680@EMVs-aPDL1 group had significantly elevated concentrations of TNF-α (399.70 ± 48.41 pg/mL) and IFN-γ (145.60 ± 15.08 pg/mL; Fig. 6C, D). The EMVs-aPDL1 group had concentrations of TNF-α (289.73 ± 30.42 pg/mL) and IFN-γ (123.78 ± 11.55 pg/mL) that were higher than the concentrations in the AB680@EMVs group (232.35 ± 16.44 and 101.30 ± 8.97 pg/mL, respectively; $P < 0.01$). Furthermore, the TNF-α and IFN-γ concentrations were lower in the EMVs-aPDL1 group than in the AB680@EMVs-aPDL1 group ($P < 0.01$ and $P < 0.05$, respectively). Thus, the additional delivery of a CD73 inhibitor in AB680@EMVs-aPDL1 amplified the efficacy of ICI treatment in this in vivo model. Effector T cells act as immune stimulators, contribute to the activation and proliferation of cytotoxic T cells, and secrete various cytokines, including IL-2, TNF-α, and IFN-γ [58]. Once activated, cytotoxic T cells destroy the tumor cells by releasing cytokines, perforins, and granzymes and by induction of apoptosis [51]. Thus, the significantly elevated intratumoral concentrations of TNF-α and IFN-γ in the AB680@EMVs-aPDL1 group may help explain the cytotoxic effects of the treatment on bladder cancer.

In vitro toxicity and in vivo biosafety

Safe treatment with low cytotoxicity against normal cells is essential for long-term clinical use. In vitro results using CCK-8 assays revealed that 24 h of treatment with AB680@EMVs-aPDL1 did not significantly affect MB49 cell viability (Fig. 7A). In addition, free AB680 had mild cytotoxic effects, which were eliminated when AB680 was combined with EMVs (Fig. 7A). Moreover, after adjusting for

differences in tumor response, no significant differences in body weight were observed between the AB680@EMVs-aPDL1, AB680@EMV, and EMV groups (Fig. 7B), suggesting that EMV-based treatments were not associated with any clear systemic toxicity during the experiment. Histological examination of the tumor specimens also failed to reveal any clearly necrotic areas in specimens from all of the treatment groups (Fig. 7C). Therefore, the AB680@EMVs-aPDL1 were found to be sufficiently safe to permit additional research regarding whether these complexes could be used as long-term therapy.

Conclusion

In summary, we created macrophage-derived EMVs that were coloaded using a CD73 inhibitor (AB680) and antibodies targeting PD-L1 (aPDL1). The AB680 was encapsulated using a co-extrusion method, and the EMVs were then conjugated to aPDL1. Our results suggest that these therapeutic nanovesicles provided excellent tumor targeting and were safe, based on in vitro and in vivo results. Moreover, simultaneous delivery of AB680 inhibited extracellular adenosine production, which allowed for activation of cytotoxic T lymphocytes and improved responses to aPDL1 treatment. Therefore, this natural nanoplatform may be a novel and promising strategy for delivering combined immunotherapy to bladder tumors.

Declarations

Ethics approval and consent to participate

Not applicable.

Consent for publication

Not applicable.

Availability of data and materials

All data generated or analyzed during this study are included in this published article.

Competing interests

The authors declare that they have no competing interests.

Funding

This work was funded by the National Natural Science Foundation of China (grant nos. 81803078, 81372756, and 81703434) and the Science and Technology Commission of Shanghai Municipality (grant no. 19ZR1408000).

Authors' contributions

QZ: methodology, investigation, and writing-original draft preparation; WD: methodology, investigation, and funding acquisition; ZQ: methodology, investigation, and data recording; QZ: methodology and investigation; CS: investigation and visualization; QY: investigation and funding acquisition; ZT: writing-review & editing, supervision, and funding acquisition; KX: conceptualization, supervision, and funding acquisition. All authors read and approved the final manuscript. QZ, WD and ZQ contributed equally.

Acknowledgements

The authors are very grateful to Dr. Sida Han for kind assistance in flow cytometry assays.

References

[1]. Witjes, J.A., et al., European Association of Urology Guidelines on Muscle-invasive and Metastatic Bladder Cancer: Summary of the 2020 Guidelines. Eur Urol, 2021. 79(1): p. 82-104.

[2]. Fernandez, M.I., et al., Epidemiology, prevention, screening, diagnosis, and evaluation: update of the ICUD-SIU joint consultation on bladder cancer. World J Urol, 2019. 37(1): p. 3-13.

[3]. Gakis, G., et al., ICUD-EAU International Consultation on Bladder Cancer 2012: Radical cystectomy and bladder preservation for muscle-invasive urothelial carcinoma of the bladder. Eur Urol, 2013. 63(1): p. 45-57.

[4]. Spiess, P.E., et al., Bladder Cancer, Version 5.2017, NCCN Clinical Practice Guidelines in Oncology. J Natl Compr Canc Netw, 2017. 15(10): p. 1240-1267.

[5]. Sternberg, C.N. and R. Sylvester, Thoughts on a systematic review and meta-analysis of adjuvant chemotherapy in muscle-invasive bladder cancer. Eur Urol, 2014. 66(1): p. 55-6.

[6]. Yuh, B.E., et al., Pooled analysis of clinical outcomes with neoadjuvant cisplatin and gemcitabine chemotherapy for muscle invasive bladder cancer. J Urol, 2013. 189(5): p. 1682-6.

[7]. Spranger, S. and T.F. Gajewski, Impact of oncogenic pathways on evasion of antitumour immune responses. Nat Rev Cancer, 2018. 18(3): p. 139-147.

[8]. Choudhury, N.J., et al., Low T-cell Receptor Diversity, High Somatic Mutation Burden, and High Neoantigen Load as Predictors of Clinical Outcome in Muscle-invasive Bladder Cancer. Eur Urol Focus, 2016. 2(4): p. 445-452.

[9]. Kandoth, C., et al., Mutational landscape and significance across 12 major cancer types. Nature, 2013. 502(7471): p. 333-339.

[10]. Tripathi, A. and E.R. Plimack, Immunotherapy for Urothelial Carcinoma: Current Evidence and Future Directions. Curr Urol Rep, 2018. 19(12): p. 109.

[11]. Powles, T., et al., Efficacy and Safety of Durvalumab in Locally Advanced or Metastatic Urothelial Carcinoma: Updated Results From a Phase 1/2 Open-label Study. JAMA Oncol, 2017. 3(9): p. e172411.

[12]. Sharma, P., et al., Nivolumab in metastatic urothelial carcinoma after platinum therapy (CheckMate 275): a multicentre, single-arm, phase 2 trial. Lancet Oncol, 2017. 18(3): p. 312-322.

[13]. Vlachostergios, P.J. and B.M. Faltas, The molecular limitations of biomarker research in bladder cancer. World J Urol, 2019. 37(5): p. 837-848.

[14]. Kavanagh, B., et al., CTLA4 blockade expands FoxP3+ regulatory and activated effector CD4+ T cells in a dose-dependent fashion. Blood, 2008. 112(4): p. 1175-83.

[15]. Allard, B., et al., Immunosuppressive activities of adenosine in cancer. Curr Opin Pharmacol, 2016. 29: p. 7-16.

[16]. Wang, L., et al., CD73 has distinct roles in nonhematopoietic and hematopoietic cells to promote tumor growth in mice. J Clin Invest, 2011. 121(6): p. 2371-82.

[17]. Allard, D., et al., Targeting the CD73-adenosine axis in immuno-oncology. Immunol Lett, 2019. 205: p. 31-39.

[18]. Leone, R.D. and L.A. Emens, Targeting adenosine for cancer immunotherapy. J Immunother Cancer, 2018. 6(1): p. 57.

[19]. Allard, B., et al., Targeting CD73 enhances the antitumor activity of anti-PD-1 and anti-CTLA-4 mAbs. Clin Cancer Res, 2013. 19(20): p. 5626-35.

[20]. Siu, L.L., et al., Preliminary phase 1 profile of BMS-986179, an anti-CD73 antibody, in combination with nivolumab in patients with advanced solid tumors. CANCER RESEARCH, 2018. 78S(13).

[21]. Stagg, J., et al., Anti-CD73 antibody therapy inhibits breast tumor growth and metastasis. Proc Natl Acad Sci U S A, 2010. 107(4): p. 1547-52.

[22]. Lawson, K.V., et al., Discovery of AB680: A Potent and Selective Inhibitor of CD73. J Med Chem, 2020. 63(20): p. 11448-11468.

[23]. Choo, Y.W., et al., M1 Macrophage-Derived Nanovesicles Potentiate the Anticancer Efficacy of Immune Checkpoint Inhibitors. ACS Nano, 2018. 12(9): p. 8977-8993.

[24]. Molinaro, R., et al., Biomimetic proteolipid vesicles for targeting inflamed tissues. Nat Mater, 2016. 15(9): p. 1037-46.

[25]. Roth, J.C., D.T. Curiel and L. Pereboeva, Cell vehicle targeting strategies. Gene Ther, 2008. 15(10): p. 716-29.

[26]. Fan, J., et al., Generation of Small RNA-Modulated Exosome Mimetics for Bone Regeneration. ACS Nano, 2020. 14(9): p. 11973-11984.

[27]. Jo, W., et al., Large-scale generation of cell-derived nanovesicles. Nanoscale, 2014. 6(20): p. 12056-64.

[28]. Lin, Q., et al., Exosome-like nanoplatform modified with targeting ligand improves anti-cancer and anti-inflammation effects of imperialine. J Control Release, 2019. 311-312: p. 104-116.

[29]. Li, Y., et al., Circular RNA is enriched and stable in exosomes: a promising biomarker for cancer diagnosis. Cell Res, 2015. 25(8): p. 981-4.

[30]. Rayamajhi, S., et al., Macrophage-derived exosome-mimetic hybrid vesicles for tumor targeted drug delivery. Acta Biomater, 2019. 94: p. 482-494.

[31]. Jadus, M.R., et al., Macrophages can recognize and kill tumor cells bearing the membrane isoform of macrophage colony-stimulating factor. Blood, 1996. 87(12): p. 5232-41.

[32]. Jang, S.C., et al., Bioinspired exosome-mimetic nanovesicles for targeted delivery of chemotherapeutics to malignant tumors. ACS Nano, 2013. 7(9): p. 7698-710.

[33]. Lunavat, T.R., et al., RNAi delivery by exosome-mimetic nanovesicles - Implications for targeting c-Myc in cancer. Biomaterials, 2016. 102: p. 231-8.

[34]. Abdolahpour, S., et al., Targeted delivery of doxorubicin into tumor cells by nanostructured lipid carriers conjugated to anti-EGFRvIII monoclonal antibody. Artif Cells Nanomed Biotechnol, 2018. 46(1): p. 89-94.

[35]. Wang, R., et al., Application of poly(ethylene glycol)-distearoylphosphatidylethanolamine (PEG-DSPE) block copolymers and their derivatives as nanomaterials in drug delivery. Int J Nanomedicine, 2012. 7: p. 4185-98.

[36]. Ye, J., et al., Vitamin E-rich Nanoemulsion Enhances the Antitumor Efficacy of Low-Dose Paclitaxel by Driving Th1 Immune Response. Pharm Res, 2017. 34(6): p. 1244-1254.

[37]. Roy, A., et al., Anticancer and immunostimulatory activity by conjugate of paclitaxel and non-toxic derivative of LPS for combined chemo-immunotherapy. Pharm Res, 2012. 29(8): p. 2294-309.

[38]. Vandeveer, A.J., et al., Systemic Immunotherapy of Non-Muscle Invasive Mouse Bladder Cancer with Avelumab, an Anti-PD-L1 Immune Checkpoint Inhibitor. Cancer Immunol Res, 2016. 4(5): p. 452-62.

[39]. Wang, L., et al., A novel alpha-enolase-targeted drug delivery system for high efficacy prostate cancer therapy. Nanoscale, 2018. 10(28): p. 13673-13683.

[40]. Guo, L., et al., Targeted delivery of celastrol to mesangial cells is effective against mesangioproliferative glomerulonephritis. Nat Commun, 2017. 8(1): p. 878.

[41]. Conner, S.D. and S.L. Schmid, Regulated portals of entry into the cell. Nature, 2003. 422(6927): p. 37-44.

[42]. Gong, C., et al., Co-delivery of autophagy inhibitor ATG7 siRNA and docetaxel for breast cancer treatment. J Control Release, 2017. 266: p. 272-286.

[43]. Kalimuthu, S., et al., A New Approach for Loading Anticancer Drugs Into Mesenchymal Stem Cell-Derived Exosome Mimetics for Cancer Therapy. Front Pharmacol, 2018. 9: p. 1116.

[44]. Corbet, C. and O. Feron, Tumour acidosis: from the passenger to the driver's seat. Nat Rev Cancer, 2017. 17(10): p. 577-593.

[45]. Tian, T., et al., Exosome uptake through clathrin-mediated endocytosis and macropinocytosis and mediating miR-21 delivery. J Biol Chem, 2014. 289(32): p. 22258-67.

[46]. Xu, S., et al., PD-L1 monoclonal antibody-conjugated nanoparticles enhance drug delivery level and chemotherapy efficacy in gastric cancer cells. Int J Nanomedicine, 2019. 14: p. 17-32.

[47]. Hatfield, S.M. and M. Sitkovsky, A2A adenosine receptor antagonists to weaken the hypoxia-HIF-1alpha driven immunosuppression and improve immunotherapies of cancer. Curr Opin Pharmacol, 2016. 29: p. 90-6.

[48]. Ohta, A., et al., A2A adenosine receptor protects tumors from antitumor T cells. Proc Natl Acad Sci U S A, 2006. 103(35): p. 13132-7.

[49]. Cibrian, D. and F. Sanchez-Madrid, CD69: from activation marker to metabolic gatekeeper. Eur J Immunol, 2017. 47(6): p. 946-953.

[50]. Ruoslahti, E., S.N. Bhatia and M.J. Sailor, Targeting of drugs and nanoparticles to tumors. J Cell Biol, 2010. 188(6): p. 759-68.

[51]. Tej, G., K. Neogi and P.K. Nayak, Caffeine-enhanced anti-tumor activity of anti-PD1 monoclonal antibody. Int Immunopharmacol, 2019. 77: p. 106002.

[52]. Ding, W., et al., Ki-67 is an independent indicator in non-muscle invasive bladder cancer (NMIBC); combination of EORTC risk scores and Ki-67 expression could improve the risk stratification of NMIBC. Urol Oncol, 2014. 32(1): p. 42.e13-9.

[53]. Bullwinkel, J., et al., Ki-67 protein is associated with ribosomal RNA transcription in quiescent and proliferating cells. J Cell Physiol, 2006. 206(3): p. 624-35.

[54]. Zou, W., J.D. Wolchok and L. Chen, PD-L1 (B7-H1) and PD-1 pathway blockade for cancer therapy: Mechanisms, response biomarkers, and combinations. Sci Transl Med, 2016. 8(328): p. 328rv4.

[55]. Flores-Santibanez, F., et al., CD73-mediated adenosine production promotes stem cell-like properties in mouse Tc17 cells. Immunology, 2015. 146(4): p. 582-94.

[56]. Bono, M.R., et al., CD73 and CD39 ectonucleotidases in T cell differentiation: Beyond immunosuppression. FEBS Lett, 2015. 589(22): p. 3454-60.

[57]. Saito, R., et al., Molecular Subtype-Specific Immunocompetent Models of High-Grade Urothelial Carcinoma Reveal Differential Neoantigen Expression and Response to Immunotherapy. Cancer Res, 2018. 78(14): p. 3954-3968.

[58]. Luckheeram, R.V., et al., CD4(+)T cells: differentiation and functions. Clin Dev Immunol, 2012. 2012: p. 925135.

Tables

Table 1. Comparison of the characteristics of EMVs, AB680@EMVs, and AB680@EMVs-aPDL1.

Nanovesicles	PDI	EE(%)	DL(ng/mg protein)*
EMVs	0.119±0.017	-	-
AB680@EMVs	0.124±0.008	68.7±4.9	0.113±0.008
AB680@EMVs-aPDL1	0.108±0.013	61.0±3.1	0.102±0.009

Data are presented as means ± standard deviations, n = 3.

*The optimal drug loading efficiency.

AB680: a CD73 inhibitor, EMVs: exosome-mimetic nanovesicles, aPDL1: monoclonal antibody targeting programmed cell death ligand 1, PDI: polydispersity index, EE: encapsulation efficiency, DL: drug loading.

Table 2. The aPDL1 contents of the EMVs-aPDL1 at various EMVs/aPDL1 ratios.

Weight ratio of EMVs to aPDL1 (mg protein/mg, w/w)	Graft ratio of aPDL1 content (%, w/w)
1.0	2.49 ± 0.18
1.5	3.81 ± 0.26
2.0	4.72 ± 0.30
2.5*	5.47 ± 0.36
3.0	5.50 ± 0.24
3.5	5.45 ± 0.19

*The 2.5 weight ratio of EMVs/aPDL1 (mg protein/mg, w/w) was the best option for constructing the EMVs-aPDL1 nanoparticles.

EMVs: exosome-mimetic nanovesicles, aPDL1: monoclonal antibody targeting programmed cell death ligand 1.

Figures

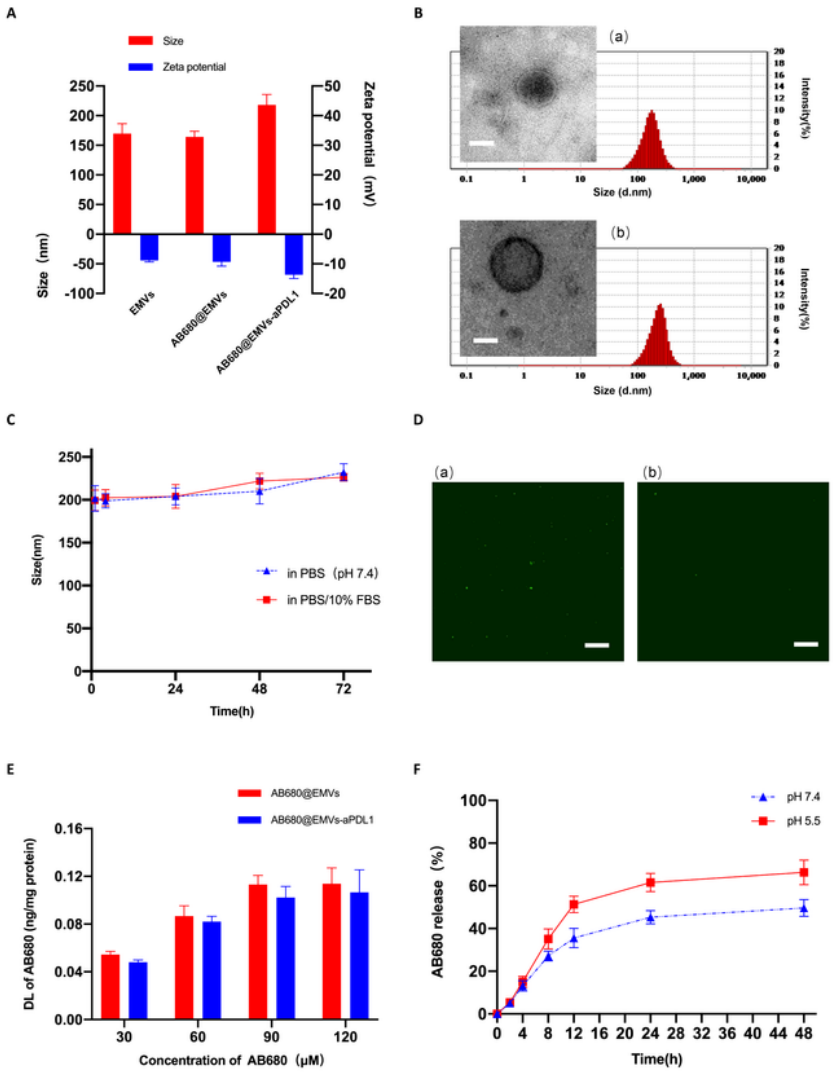

Figure 1

Characterization of AB680@EMVs-aPDL1. (A) Particle sizes and zeta potential of EMVs, AB680@EMVs, and AB680@EMVs-aPDL1 determined using DLS. (B) The TEM images and size distributions of (a) AB680@EMVs and (b) AB680@EMVs-aPDL1 (scale bar: 100 nm). (C) Time-based changes in the size stability of AB680@EMVs-aPDL1 in phosphate-buffered saline (pH 7.4) and 10% fetal bovine serum. (D) Microscopic images of AB680@EMVs-aPDL1 stained using FITC-labeled secondary antibodies showing

(a) EMVs conjugated with aPDL1 and (b) unconjugated EMVs incubated with secondary antibodies as a control (scale bar: 50 μm). (E) Drug loading of AB680 into EMVs and aPDL1-EMVs at different concentrations. (F) Profiles of AB680 release from AB680@EMVs-aPDL1 at pH 5.5 and pH 7.4 (mean ± standard deviation, n = 3). AB680: CD73 inhibitor, EMVs: exosome-mimetic nanovesicles, aPDL1: monoclonal antibody targeting programmed cell death ligand 1, DLS: dynamic light scattering, TEM: transmission electron microscopy, FITC: fluorescein isothiocyanate

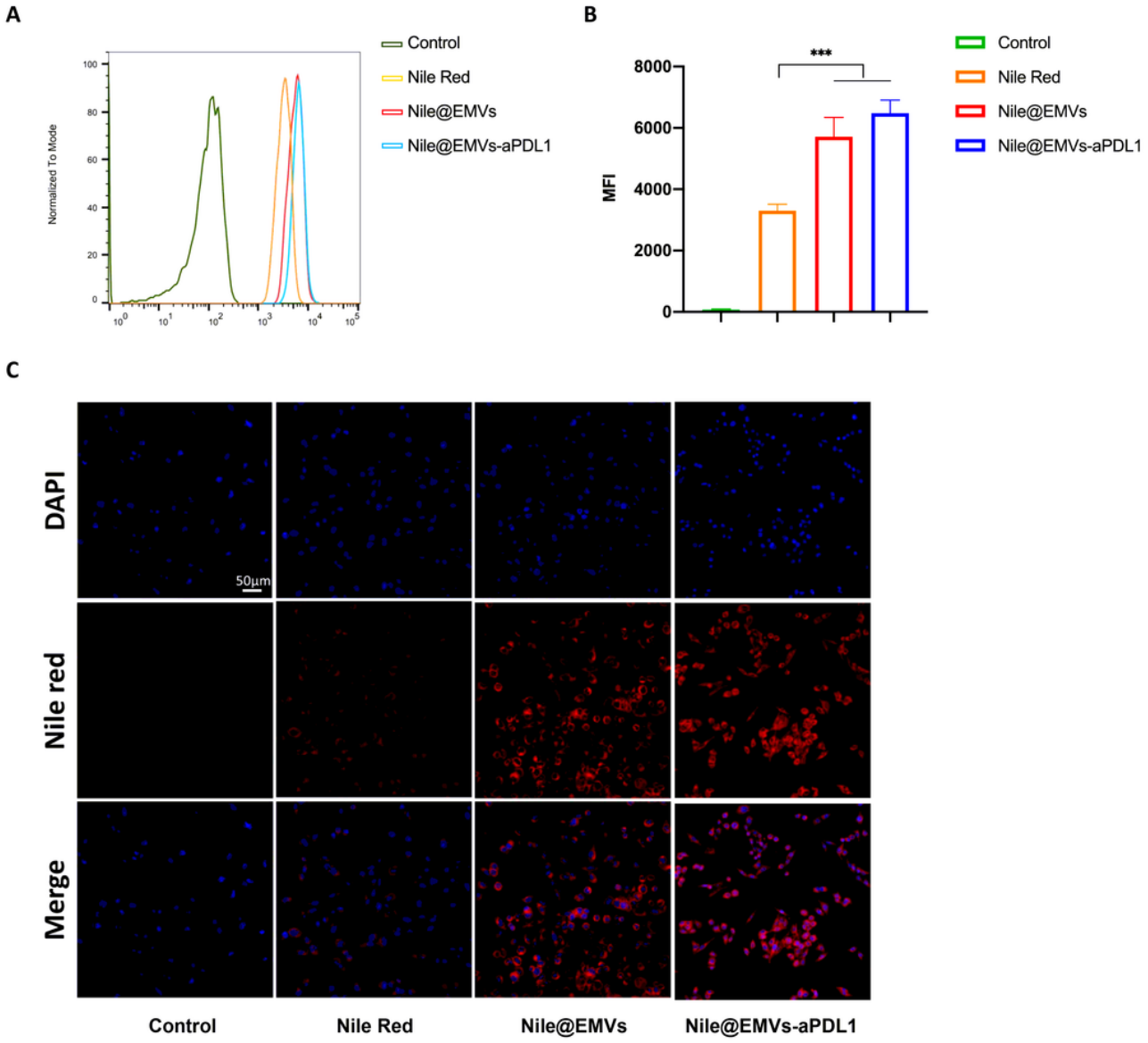

Figure 2

Cellular uptake of Nile red in different EMVs. (A) Flow cytometry data showing Nile red uptake by MB49 cells. (B) Quantitative analysis of the mean fluorescence intensity from Nile red in MB49 cells (mean ± standard deviation, n = 3). (C) Confocal microscopy images of MB49 cells after 2 h of incubation with phosphate-buffered saline, Nile red, Nile@EMVs, and Nile@EMVs-aPDL1. Blue signals represent cell

nuclei and red signals represent Nile red staining (scale bar: 50 μm). EMVs: exosome-mimetic nanovesicles, aPDL1: a monoclonal antibody to programmed cell death ligand 1, ***P < 0.001.

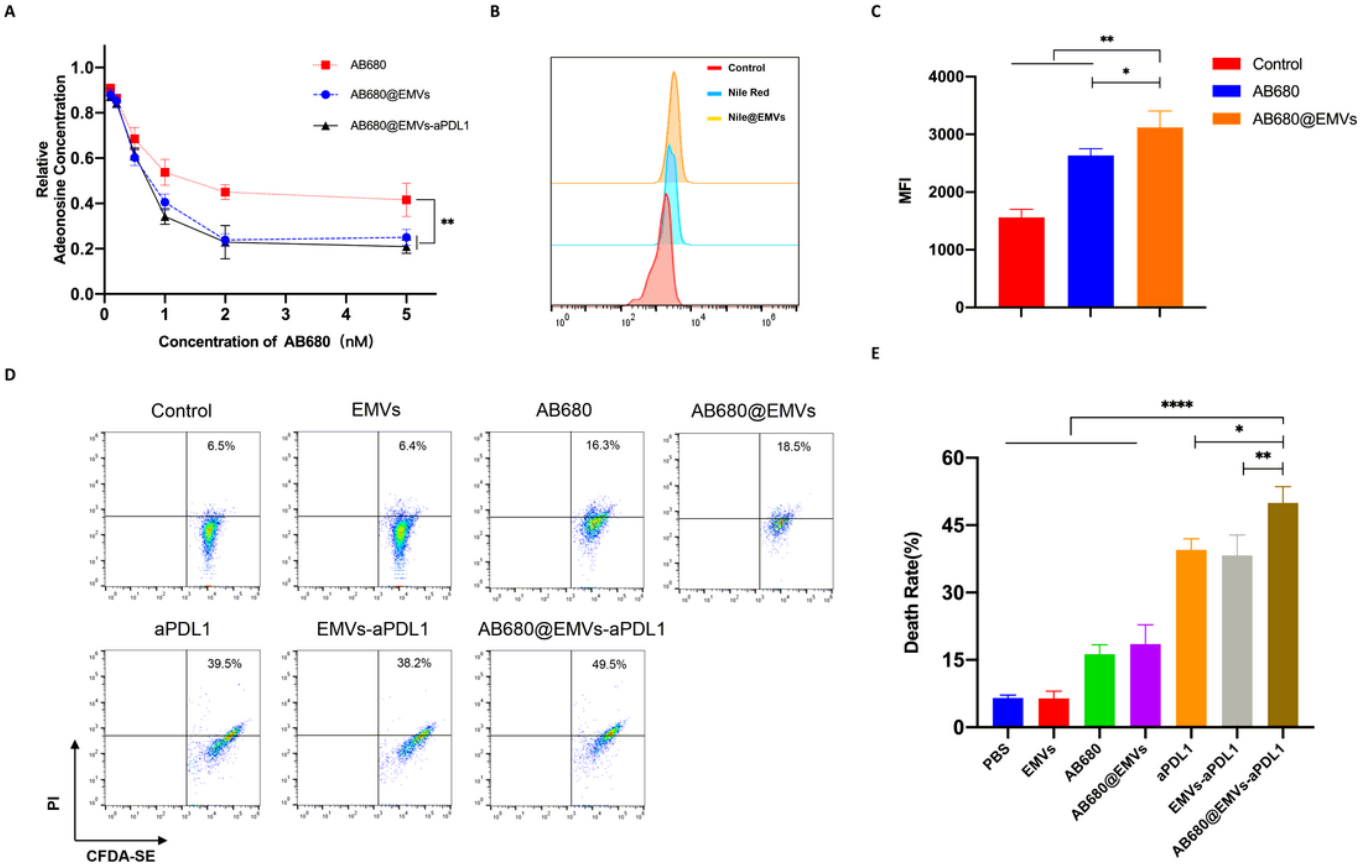

Figure 3

In vitro antitumor effects of AB680@EMVs-aPDL1. (A) The CD73 inhibitory activity was measured based on the inhibition of extracellular adenosine production. (B) Flowcytometry analysis of CD69 expression to evaluate activation of CD8+ T-cells. (C) Mean fluorescence intensity statistics for CD69 expression in CD8+ T-cells. (D) In vitro cytotoxicity was evaluated using a co-culture of CFDA-SE labeled MB49 cells and splenocytes. (E) The death rate of bladder cancer cells was evaluated based on the rate of PI-positive and CFDA-SE-positive cells (mean ± standard deviation, n = 3). AB680: a CD73 inhibitor, EMVs: exosome-mimetic nanovesicles, aPDL1: a monoclonal antibody to programmed cell death ligand 1, CFDS-SE: carboxyfluorescein diacetate succinimidyl ester, PI: propidium iodide, *p < 0.05, **p < 0.01, ****p < 0.0001.

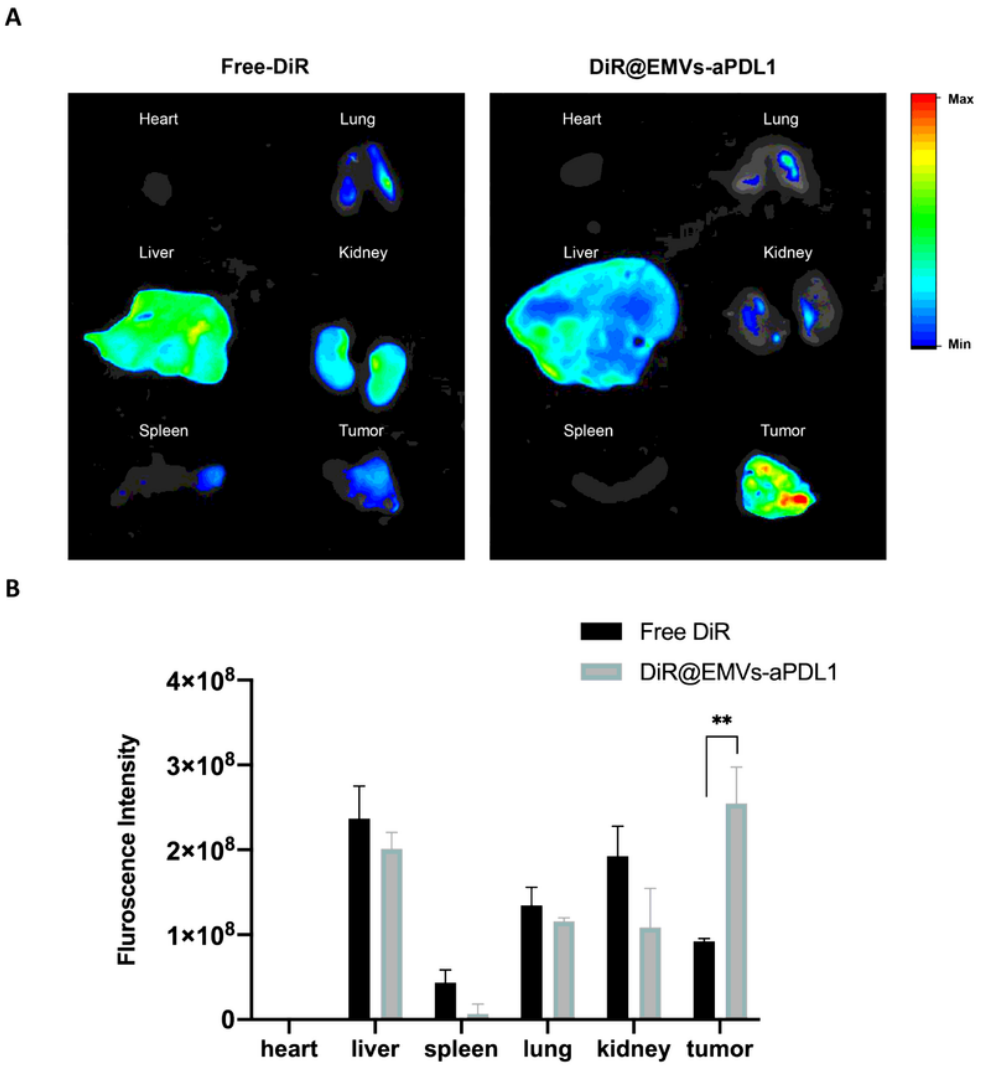

Figure 4

In vivo biodistribution. (A) Representative fluorescence images showing biodistribution in tumor tissues and major organs (heart, liver, spleen, lungs, and kidneys) that were removed from tumor-bearing C57BL/6J mice at 24 h after injection with free DiR and DiR@EMVs-aPDL1 via the tail vein. (B) Accumulated fluorescence signals in the organs and tumor tissues evaluated using in vivo imaging (mean ± standard deviation, n = 6). DiR: 1.1'-dioctadecyltetramethyl indotricarbocyanine iodide, EMVs: exosome-mimetic nanovesicles, aPDL1: a monoclonal antibody to programmed cell death ligand 1, **p < 0.01.

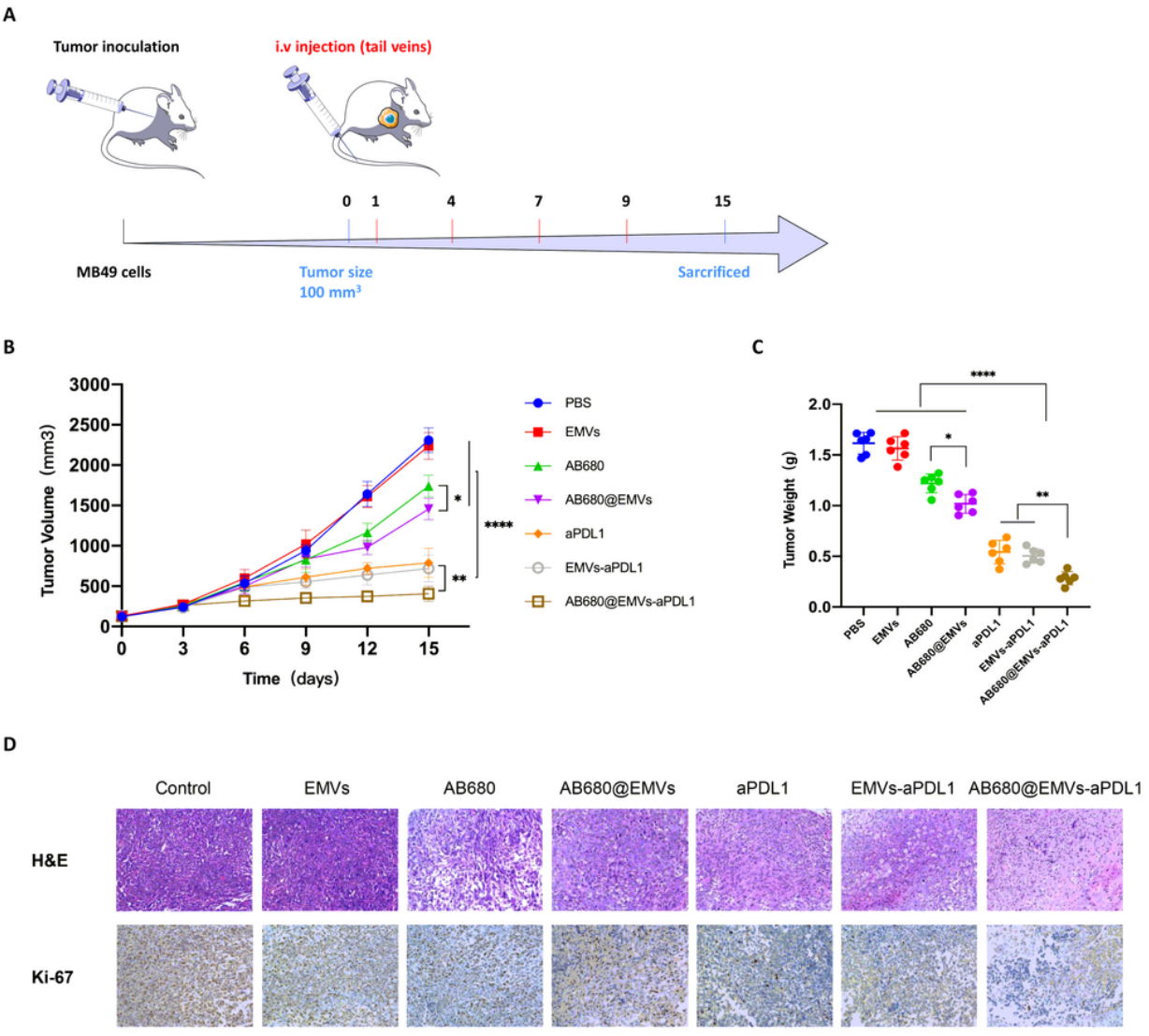

Figure 5

In vivo anti-tumor effects of AB680@EMVs-aPDL1 in tumor-bearing C57BL/6J mice. (A) Schematic illustration of the in vivo study; the concentration of AB680 and aPDL1 were 10 mg/kg and 5 mg/kg, respectively. (B) Tumor volume growth curves for mice that received the different treatments. (C) Tumor weights were measured after excision from each group (mean ± standard deviation, n = 6). (D) Hematoxylin and eosin staining (200×) and immunohistochemical staining for Ki67 (200×) using the tumor slices. AB680: a CD73 inhibitor, EMVs: exosome-mimetic nanovesicles, aPDL1: a monoclonal antibody to programmed cell death ligand 1, *p < 0.05, **p < 0.01, ****p < 0.0001.

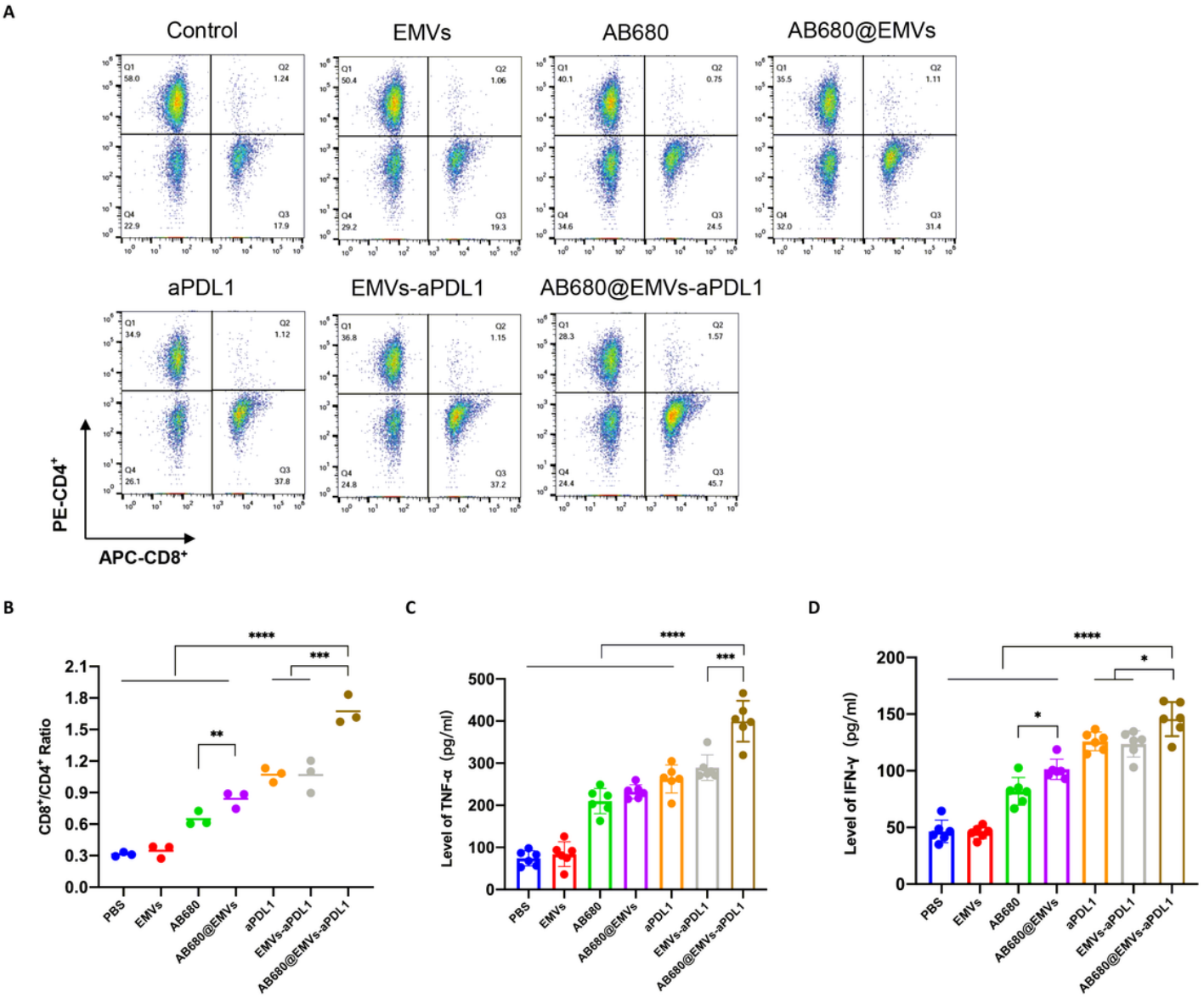

Figure 6

In vivo effects of combination immunotherapy. (A) Flow cytometry showing the CD8+/CD4+ T-cell ratio. (B) The CD8+/CD4+ ratio after immune stimulation in all groups (n = 3). (C,D) The TNF-α and IFN-γ concentrations in the tumor tissues from the various groups (mean ± standard deviation, n = 6). TNF-α: tumor necrosis factor alpha, IFN-γ: interferon gamma, *P < 0.5, **P < 0.01, ***P < 0.001, ****P < 0.0001.

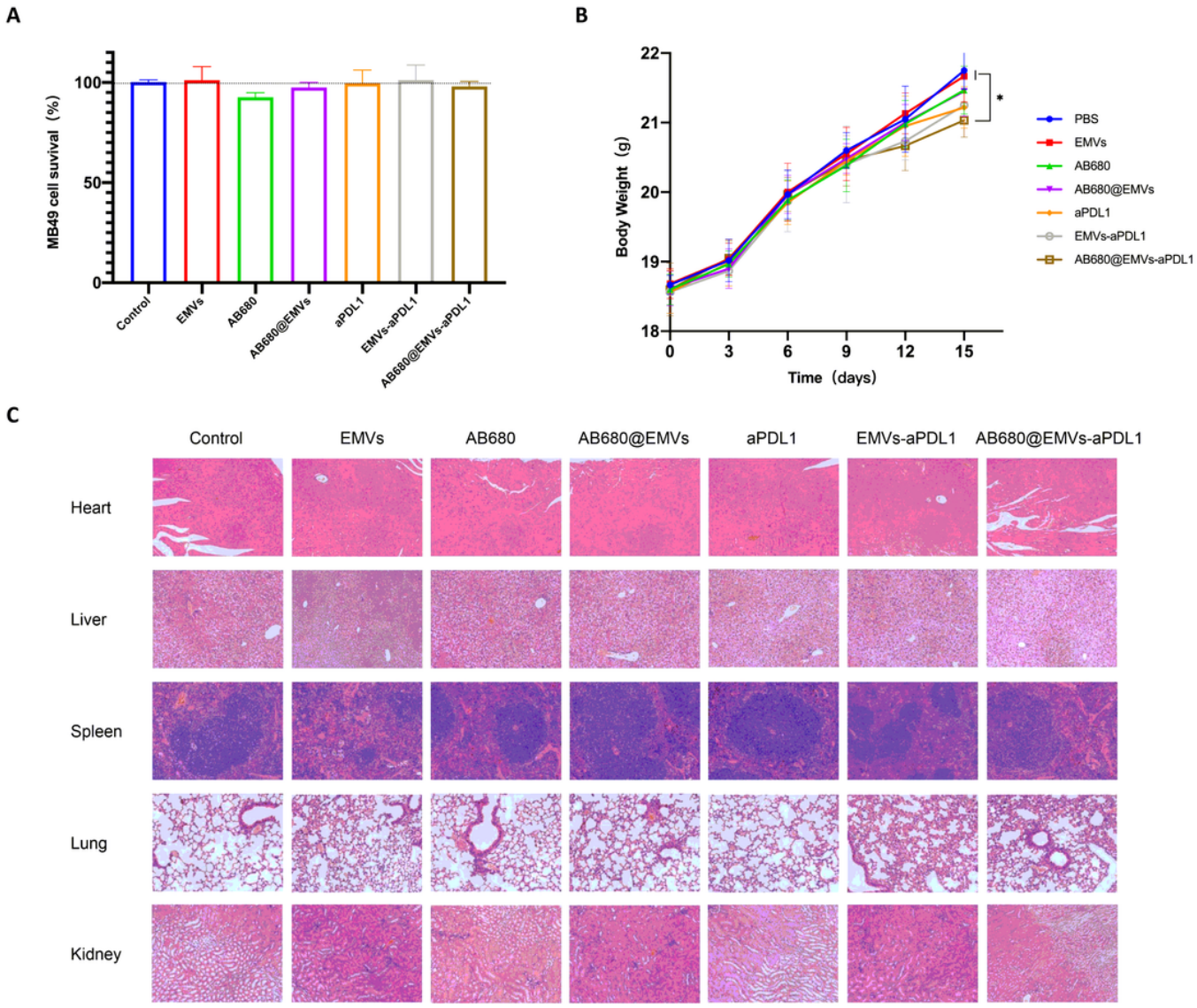

Figure 7

In vitro and in vivo safety assessments for each group. (A) The CCK8 assay revealed that the EMVs with AB680 and/or aPDL1 had limited cytotoxic effects on MB49 cells (mean ± standard deviation, n = 3). (B) Body weight changes in MB49 tumor-bearing mice according to various treatments (mean ± standard deviation, n = 6). (C) Hematoxylin and eosin staining (200×) of major organs from MB49 tumor-bearing mice after immunotherapy revealed normal morphology. AB680: a CD73 inhibitor, EMVs: exosome-mimetic nanovesicles, aPDL1: a monoclonal antibody to programmed cell death ligand 1, *p < 0.05 vs. phosphate-buffered saline and EMVs.

Supplementary Files

This is a list of supplementary files associated with this preprint. Click to download.

- Onlines.png